Human Molecular Genetics, 2018, Vol. 27, No. 18 3233–3245

doi: 10.1093/hmg/ddy218
Advance Access Publication Date: 14 June 2018
Original Article

ORIGINAL ARTICLE

Pathogenic variant in *EPHB4* results in central conducting lymphatic anomaly

Dong Li[1], Tara L. Wenger[2], Christoph Seiler[3], Michael E. March[1], Alvaro Gutierrez-Uzquiza[1], Charlly Kao[1], Elizabeth Bhoj[1], Lifeng Tian[1], Misha Rosenbach[4], Yichuan Liu[1], Nora Robinson[1], Mechenzie Behr[1], Rosetta Chiavacci[1], Cuiping Hou[1], Tiancheng Wang[1], Marina Bakay[1], Renata Pellegrino da Silva[1], Jonathan A. Perkins[5], Patrick Sleiman[1,6] Michael A. Levine[6,7], Patricia J. Hicks[6], Maxim Itkin[8], Yoav Dori[8] and Hakon Hakonarson[1,6,9,*]

[1]Center for Applied Genomics, The Children's Hospital of Philadelphia, Philadelphia, PA 19104, USA, [2]Division of Craniofacial Medicine, Seattle Children's Hospital, Seattle, WA 98105, USA, [3]Zebrafish core, The Children's Hospital of Philadelphia, Philadelphia, PA 19104, USA, [4]Department of Dermatology, University of Pennsylvania School of Medicine, Philadelphia, PA 19104, USA, [5]Division of Otolaryngology–Head and Neck Surgery, Seattle Children's Hospital, Seattle, WA 98105, USA, [6]Department of Pediatrics, University of Pennsylvania School of Medicine, Philadelphia, PA 19104, USA, [7]Division of Endocrinology and Diabetes, [8]Center for Lymphatic Imaging and Interventions and [9]Divisions of Human Genetics and Pulmonary Medicine, The Children's Hospital of Philadelphia, Philadelphia, PA 19104, USA

*To whom correspondence should be addressed at: Center for Applied Genomics, Abramson Research Building, Suite 1216B, 3615 Civic Center Boulevard, Philadelphia, PA 19104-4318, USA. Tel: +1 2674260088; Fax: +1 267260363; Email: hakonarson@email.chop.edu

Abstract

Central conducting lymphatic anomaly (CCLA) is one of the complex lymphatic anomalies characterized by dilated lymphatic channels, lymphatic channel dysmotility and distal obstruction affecting lymphatic drainage. We performed whole exome sequencing (WES) of DNA from a four-generation pedigree and examined the consequences of the variant by transfection of mammalian cells and morpholino and rescue studies in zebrafish. WES revealed a heterozygous mutation in *EPHB4* (RefSeq NM_004444.4; c.2334 + 1G>C) and RNA-Seq demonstrated that the *EPHB4* mutation destroys the normal donor site, which leads to the use of a cryptic splice donor that results in retention of the intervening 12-bp intron sequence. Transient co-expression of the wild-type and mutant EPHB4 proteins showed reduced phosphorylation of tyrosine, consistent with a loss-of-function effect. Zebrafish *ephb4a* morpholino resulted in vessel misbranching and deformities in the lymphatic vessel development, indicative of possible differentiation defects in lymphatic vessels, mimicking the lymphatic presentations of the patients. Immunoblot analysis using zebrafish lysates demonstrated over-activation of mTORC1 as a consequence of reduced EPHB4 signaling. Strikingly, drugs that inhibit mTOR signaling or RAS-MAPK signaling effectively rescued the misbranching phenotype in a comparable manner. Moreover, knock-in of *EPHB4* mutation in HEK293T cells also induced

Received: January 6, 2018. **Revised:** May 24, 2018. **Accepted:** June 4, 2018

mTORC1 activity. Our data demonstrate the pathogenicity of the identified *EPHB4* mutation as a novel cause of CCLA and suggesting that ERK inhibitors may have therapeutic benefits in such patients with complex lymphatic anomalies.

Introduction

The lymphatic system is essential for maintaining extracellular and intravascular fluids, immune surveillance and defense, and small intestine dietary fat absorption (1). Development of this complex network, which performs such varied functions, requires highly regulated coordination of cell proliferation, migration, differentiation and cell–cell communication. New insights into lymphangiogenesis, lymphatic development and lymphatic vasculature remodeling have emerged through recent studies, suggesting that perturbations in the PI3K/mTOR and RAS/MAPK signaling pathways underlie persistent lymphatic dysfunction and disease (1–5). Gain-of-function mutations in *AKT1* and *PIK3CA*, resulting in elevated mTORC1 activity, have been reported in lymphatic malformations associated with syndromes, such as Proteus syndrome (OMIM 176920), CLOVES syndrome (OMIM 612918) and Klippel-Trenaunay-Weber syndrome (OMIM 149000), which have lymphatic disruption and overgrowth (6–8). Mutations in *KRAS*, *HRAS*, *BRAF*, *RAF1*, *PTPN11* and *SOS1*, resulting in dysregulated RAS pathway activity, cause lymphedema in relation with lymphangiectasia in Noonan syndrome (OMIM 163950), Costello syndrome (OMIM 218040) and cardiofaciocutaneous syndrome (OMIM 115150) (9–14).

Central conducting lymphatic anomaly (CCLA) is one of the complex lymphatic anomalies characterized by dilated lymphatic channels, lymphatic channel dysmotility and distal obstruction affecting lymphatic drainage (15). First described by Trenor III and Chaudry (15), and Clemens *et al.* (16), CCLA was classified as channel-type lymphatic malformation (17) by the International Society for the Study of Vascular Anomalies (ISSVA), presenting significant overlapping patterns of clinical symptoms with its closely related diagnosis—generalized lymphatic anomaly (GLA), including but not limited to chylothorax, chylous ascites, leakage or reflux of lymph fluid and extremity swelling. Here we report the identification of a heterozygous mutation of *EPHB4*, the gene encoding Ephrin type-B receptor 4 that was recently reported to be responsible for nonimmune hydrops fetalis and capillary malformation-arteriovenous malformation (18,19), in a four-generation family pedigree, and extend the spectrum of genes involved in lymphatic anomaly. Remarkably, in zebrafish study lymphatic vessel misbranching and developmental deformities resulting from *ephb4a* morpholino (MO) can be effectively rescued by mTOR inhibitors and MEK inhibitors.

Results

Clinical presentations and family history

The proband has a lifelong history of complex lymphovascular disease manifesting primarily as a right-sided chylous effusion (Fig. 1A and A′). He is a Caucasian male born to a non-consanguineous couple at 39.5 weeks gestation following a pregnancy complicated by fetal hydrops. He was intubated for 4 weeks due to respiratory failure. Near complete opacifications of his lungs were noted on chest X-ray at birth. After extubation he developed large pleural effusions. In order to elucidate the reason for his respiratory failure and lung opacifications, an open right lung biopsy at 4 months of age identified histologically abnormal large lymphatic structures, which was given the diagnosis of ‘pulmonary lymphangiomatosis’. At 18 months of age he had surgery to repair an undescended testicle and bilateral esotropia which was uncomplicated. He gradually improved from 18 months to 2 years of age and was able to wean off of oxygen. At 2 years of age he underwent a second surgery for ongoing strabismus, which was complicated by bilateral orbital cellulitis with multiple pathogens. Due to the unusual and severe nature of his orbital cellulitis, he was suspected to have an immunocompromised state. He did well from 3 to 8 years of age with the exception of poor growth at the fifth percentile for age. Attempted liberalization of diet resulted in diarrhea with fat-rich foods. He was completely off of oxygen from age 3 to 6, but required oxygen again beginning at age 6 when his chylothoraces returned.

At 9 years of age, he had significant worsening of chylothoraces and ongoing weight loss despite nasogastric feedings with Portagen overnight. Due to escalating respiratory symptoms at age 10, bilevel positive airway pressure (BiPAP) was initiated during sleep. By age 11 his right-sided chylothroax had become very large, and thoracentesis was performed. Approximately 2 l of chylous effusion was drained with immediate improvement in his breathing. However, the fluid re-accumulated within 12 h with a significant drop in his post-procedure albumin. Shortly after this, he was listed for lung transplantation. An operative lymphangiogram at this time revealed retrograde flow of contrast in lymphatics into retroperitoneum, abdomen, neck, mediastinum and possibly bronchi. Treatment with interferon alpha 2b, celecoxib and thalidomide did not result in any improvement. By age 11 he required oxygen at all times. He was transitioned to total parenteral nutrition for 18 months from 10 to 11.5 years of age, during which time he had significant improvement in his growth. He was transitioned back to oral nutrition, with a low-fat diet and attempt to supplement with MCT oil.

At 16 years of age he developed pulmonary edema when took an international flight, despite wearing oxygen during the flight. Chest X-ray during this time was stable and showed large right-sided opacity. During his teenage years, he also developed prominence of the veins on his lower extremities, which have gradually worsened since that time.

Pulmonary function tests at age 24 revealed total lung capacity at 59% predicted, vital capacity 58% predicted and have remained stable since that time. Echocardiogram at age 24 was normal. He has never had bony involvement and no bony abnormalities have been noted on radiographs. At age 24 years, magnetic resonance (MR) lymphangiography with gadolinium-based contrast demonstrated high pulmonary water signal and abnormal retrograde pulmonary lymphatic perfusion of the right lung as well as abnormal central lymphatic anatomy, suggestive of absent or dysfunctional lymphatic valves (Fig. 1A″). There was proliferation of many lymphatic channels in the retroperitoneum, around the spine and in the lungs. The lymphatic channels were dysfunctional and the flow was not normal after injection of lymph nodes with radioactive tracer. Maximal intensity projection (MIP) of dynamic contrast magnetic resonance lymphangiogram (DCMRL) showed retroperitoneal masses and dilated and tortuous thoracic duct with retrograde perfusion of the right lung (Fig. 1A‴). Careful review of his clinical history and images subsequently rectified his diagnosis to CCLA based on 2015 ISSVA classification of vascular anomalies (17).

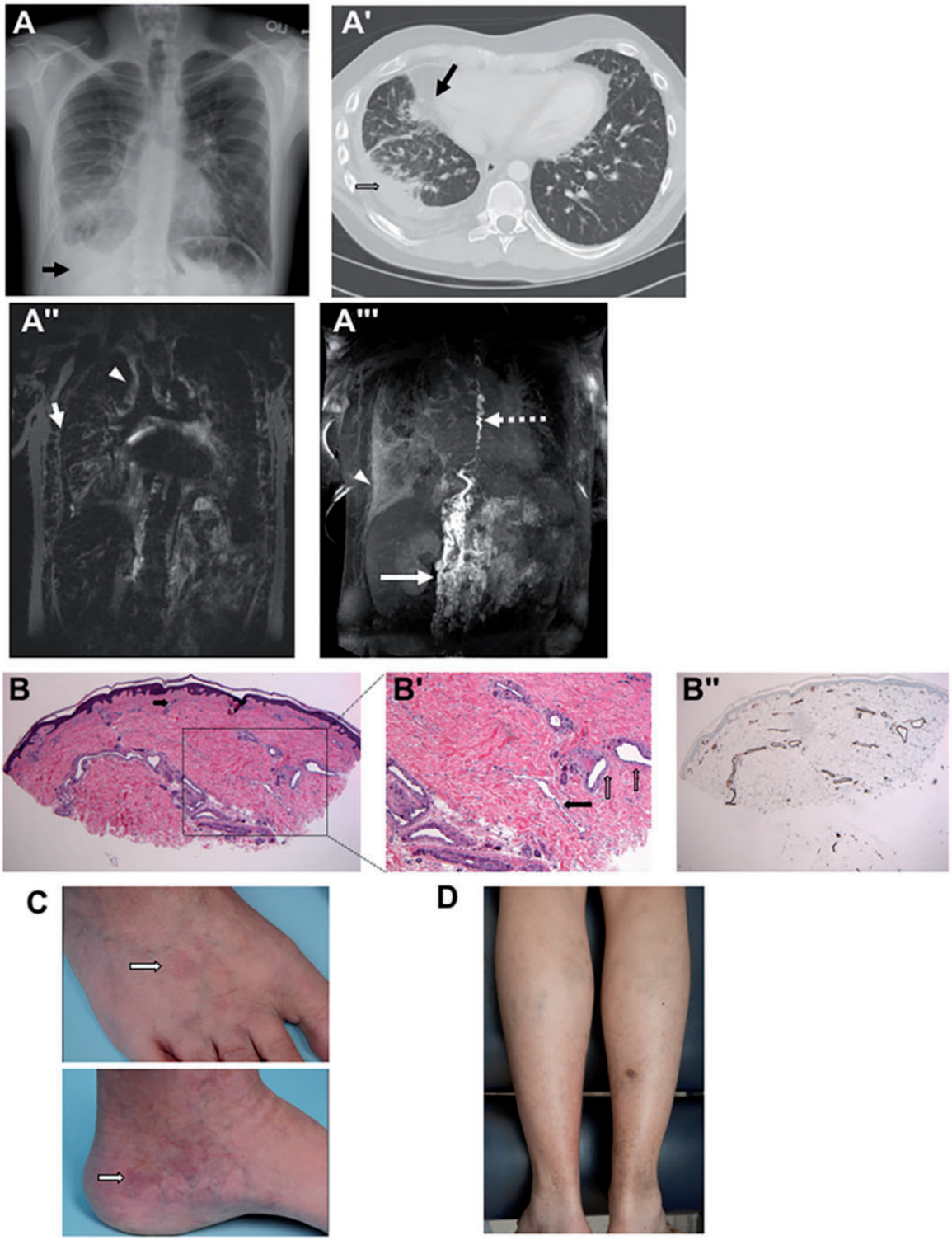

Figure 1. Clinical images and skin histopathology in patients with lymphatic anomalies. (**A**) Chest radiograph of the proband shows prominent interstitial lung markings with a right-sided pleural effusion (arrow) at 24 years of age. (**A′**) Chest CT scan of the proband shows right-sided pleural effusion (open arrow) and ground glass opacifications (black arrow) at 23 years old. (**A″**) T2-weighted MRI demonstrating high peribronchial (arrow) and pulmonary interstitial signal (arrowhead). (**A‴**) MIP of DCMRL showing retroperitoneal masses (arrow) dilated and tortuous thoracic duct (TD) (dashed arrow) with retrograde perfusion of the right lung (arrow head). (**B** and **B′**) Skin histopathology of mother of proband demonstrates a markedly increased number of dermal vascular structures. Both dilated lymphatic channels and venules/capillaries are noted (B, hematoxylin and eosin, 40×, black arrow indicates capillary in the superficial reticular dermis; B′, hematoxylin and eosin, 100×, black arrow is pointing at a dilated lymphatic channel and open vertical arrows are pointing at dilated venules). (**B″**) The dilation and thickness of venolymphatic channels stains positive for CD31 (40×), with a subset also positive for D2–40 (data not shown). (**C**) Faint, vaguely reticulated matted telangiectatic patch on the medial left foot of mother of proband, along with scattered varicosities. The dorsal foot shows a similar faint telangiectatic patch. White arrow is pointing at a telangiectatic patch in both clinical images. (**D**) Photograph of posterior calves of proband demonstrating discoloration and stasis dermatitis suggestive of longstanding venous insufficiency. Of note, the lesion on the right posterior calf is partially healed biopsy site. The biopsy site took several weeks longer to heal completely than would be anticipated, further supportive of venous insufficiency.

Family history was significant for multiple affected family members (Fig. 2A). Significant swelling of the lower extremities with superficial clots has been a consistent feature in most of affected family members, with the exception of individual II-8, grandaunt of the proband, who passed away at age 4. She had significant abdominal distension and edema in photographs, but no hospital records or photographs of the lower extremities are available to determine whether there was involvement of the lower extremities. Skin biopsy of the left lower extremities of the proband's mother demonstrated markedly increased dermal vascular structures consistent with a lymphatic and vascular malformation (Fig. 1B, B′ and B″) and her skin was noted to have some subtle and nonspecific telangiectatic patches (Fig. 1C). The other affected family members had lower extremities that were similar in appearance but no biopsies were available. Additionally, there was a presumed affected pregnancy in which a stillbirth baby was affected by hydrops (III-6). There were several individuals with prominent abdominal involvement, most prominently affecting III-7, IV-6, III-9. Mother of the proband, III-3, has required diuretic treatment for abdominal distension. Female family members, most dramatically mother of the proband (III-3) have had dysfunctional uterine bleeding requiring multiple uterine ablations. Her symptoms were much worse during pregnancy, and she also had massive postpartum hemorrhage resulting in transfer to the medical intensive care unit. Coagulopathy with multiple blood clots, despite normal hypercoagulability workup, was seen in individuals II-2, II-3, II-5, III-3, III-5 and III-7. There was variability in the age and severity of symptoms, with two individuals with fetal hydrops (IV-3 and III-6), severe involvement in early childhood in II-7 and III-7, and other affected individuals who were asymptomatic until adolescence. Venous stasis was a consistent and prominent feature in all affected family members who survived to adolescence (Fig. 1D). All affected family members have had significant morbidity related to their symptoms. Unaffected family members have had no swelling of the lower extremities, blood clots or abdominal distension. There is no recognized consanguinity.

In summary, his family history is notable for edema of lower extremities, venous stasis and variable chylous effusion in his mother, maternal uncle and aunts, maternal grandfather, maternal granduncle and grandaunts, as well as maternal great-grandmother. Six affected family members and nine unaffected family members provided samples for analysis.

Identification of *EPHB4* mutation in CCLA patient

The pedigree suggested an autosomal dominant mode of inheritance (Fig. 2A). We performed whole exome sequencing (WES) on the proband and healthy sister, both parents, one unaffected maternal aunt, as well as the affected maternal grandfather, who provided the most effective baseline data. After the WES data filtering strategy (as described in Materials and Methods), only four dominant candidates were survived (Supplementary Material, Table S1). A c.2334+1G>C substitution in *EPHB4* gene, previously implicated in a pathway for venous and lymphatic cell fate determination, was identified as the most likely candidate. Cosegregation of the mutation with phenotype was confirmed by Sanger sequencing, which demonstrated the presence of the heterozygous splicing variant in the six affected individuals and absence of the mutation in nine unaffected family members (Fig. 2A). Furthermore, the mutation was absent from the 1000 Genomes Project, COSMIC v80, ESP6500SI, gnomAD dataset with >120 000 exomes, and additional exome-sequence data from more than 4000 samples that we had previously sequenced in our in-house database (20, 21). RNA-Seq with skin biopsies obtained from the proband demonstrated that the *EPHB4* splice-altering mutation leads to use a cryptic splice donor that causes the retention of the intervening 12 bp of the intron (Fig. 2B) and leads to an in-frame insertion of four amino acids (p.L778_G779insLMLG) in the highly conserved catalytic loop of protein kinase domain (Fig. 2C), which was also confirmed by Sanger sequencing of *EPHB4* cDNA (Fig. 2D).

Functional evaluation of the insertion of four amino acids in the protein kinase domain of EPHB4

Previous reports showed that stimulation of EPHB4 receptors by Ephrin B2 through cell–cell contact induces receptor autophosphorylation (22). To determine if the insertion affects the catalytic activity of the protein, expression constructs containing the wild-type and mutant versions of *EPHB4* were generated. Transfection of the wild-type *EPHB4* cDNA into HEK293T cells resulted in constitutive tyrosine phosphorylation of the protein (Fig. 3A). In contrast, dramatically lower phosphorylation of the mutant EPHB4 was observed (Fig. 3A). As previously reported in hydrops fetalis (19), transfection of mixtures of the wild-type and mutant into HEK293T cells resulted in reduced phosphorylation, roughly in proportion to the amount of mutant transfected (Fig. 3A). The high level of constitutive phosphorylation in HEK293T cells made it impossible to examine the impact of the mutation on stimulation-induced phosphorylation. A previous report utilizing the human A375 melanoma cell line showed Ephrin-B2, the natural ligand of EPHB4, induced phosphorylation of exogenously expressed EPHB4 (23). We therefore performed a follow-up experiment in A375 cells to determine if the mutation causes differences in ligand-induced phosphorylation. Transfection of EPHB4 into the human A375 melanoma cell line resulted in far less constitutive phosphorylation of the wild-type (Fig. 3B). Stimulation of the transfected cells with Ephrin-B2 resulted in induction of phosphorylation of the wild-type, but not the mutant EPHB4 (Fig. 3B). These results suggest that the four amino-acid insertion caused by the splice-altering mutation severely impacts the kinase activity of the mutant EPHB4, consistent with a loss-of-function (LoF) effect.

Injection of *ephb4a* morpholinos results in lymphatic misbranching phenotype that is rescued by mTORC1 and MEK inhibitors

To evaluate the functional consequences of the *EPHB4* variant, we injected *ephb4a* MO antisense oligonucleotides in zebrafish that inhibits the same splice junction of exon 13 as identified in the patients. Experiments were conducted in the pan-endothelial tg(fli1: EGFP) transgenic line, in which the blood and lymphatic vasculature is marked by EGFP expression (24). During the establishment of the vasculature we observed a general expansion and fusion of vessels at the caudal vascular plexus peaking at 54 hours post fertilization (hpf) in over 50% of the MO injected larvae (Fig. 4A, B and E) (4 experiments with 225 animals, $P < 0.001$). At 4 days post fertilization (dpf), the stage when the lymphatic system has started to form (25), we detected lateral aberrant and excess branching of newly forming lymphatic vessels (identified by location and thin morphology) and intersomitic blood vessels in about 46.3% of the injected larvae (Fig. 4C–E, 6 experiments, 259 animals, $P < 4E-08$)

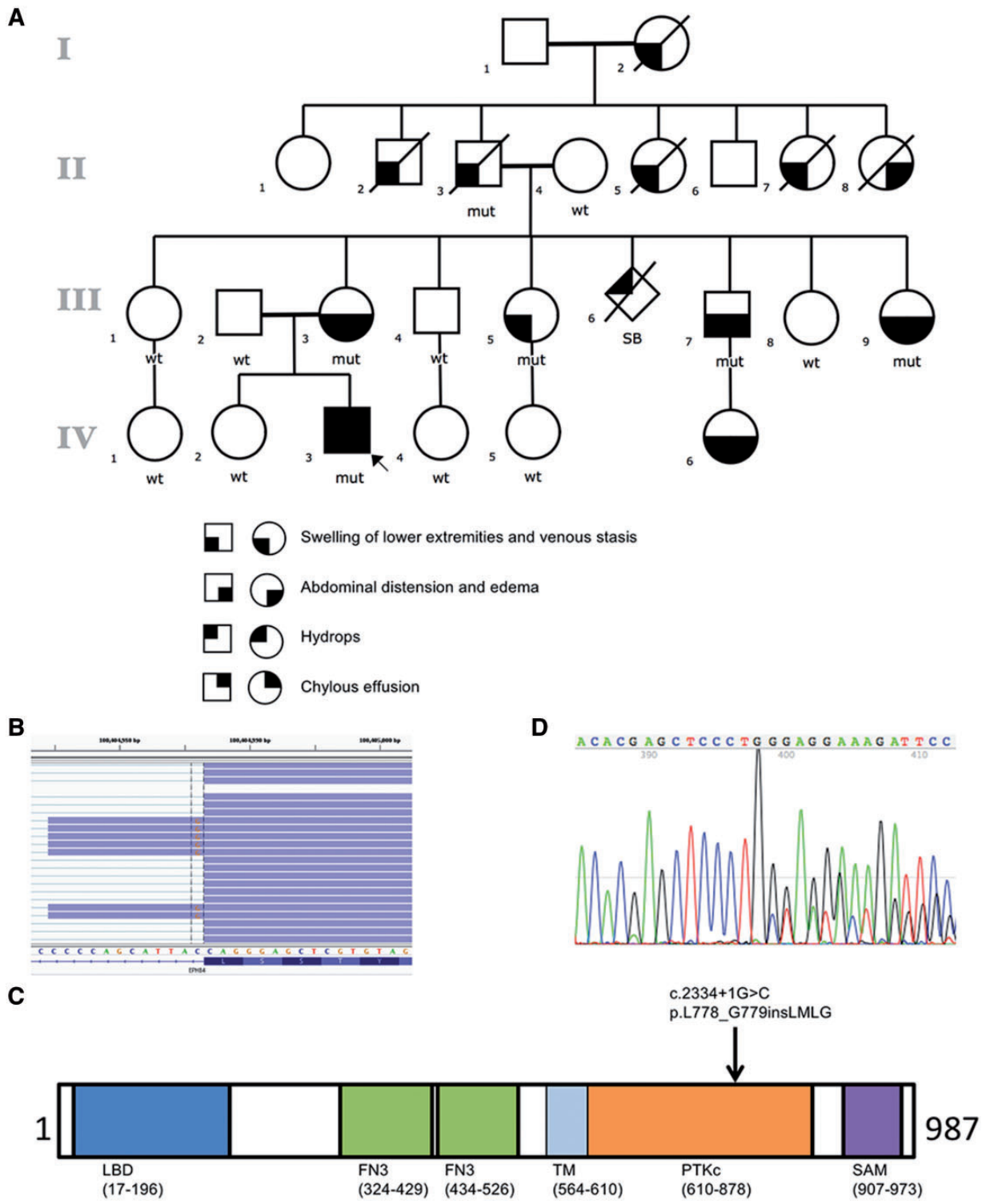

Figure 2. Identification of mutation in *EPHB4*. (**A**) Pedigree of studied family and cosegregating pattern of the *EPHB4* mutation. The open circles denote unaffected females and the open squares denote unaffected males; the solid figures indicate affected subjects. *EPHB4* genotypes are noted beneath the symbol for each subject from whom DNA was available for testing. (**B**) RNA-Seq demonstrates *EPHB4* splice-altering mutation destroys the normal donor site, which leads to the use of a cryptic splice donor (the coding strand of *EPHB4* corresponds to the chromosome's reverse strand) that causes the retention of the intervening 12 bp of the intron. (**C**) Schematic of EPHB4 protein showing conserved domains and variant identified in the affected individuals. Abbreviations are as follows: LBD, ligand binding domain; FN3, fibronectin type 3 domain; TM, transmembrane domain; PTKc, catalytic domain of the protein tyrosine kinases; SAM, sterile alpha motif. (**D**) The in-frame insertion was confirmed by Sanger sequencing of cDNA from patient.

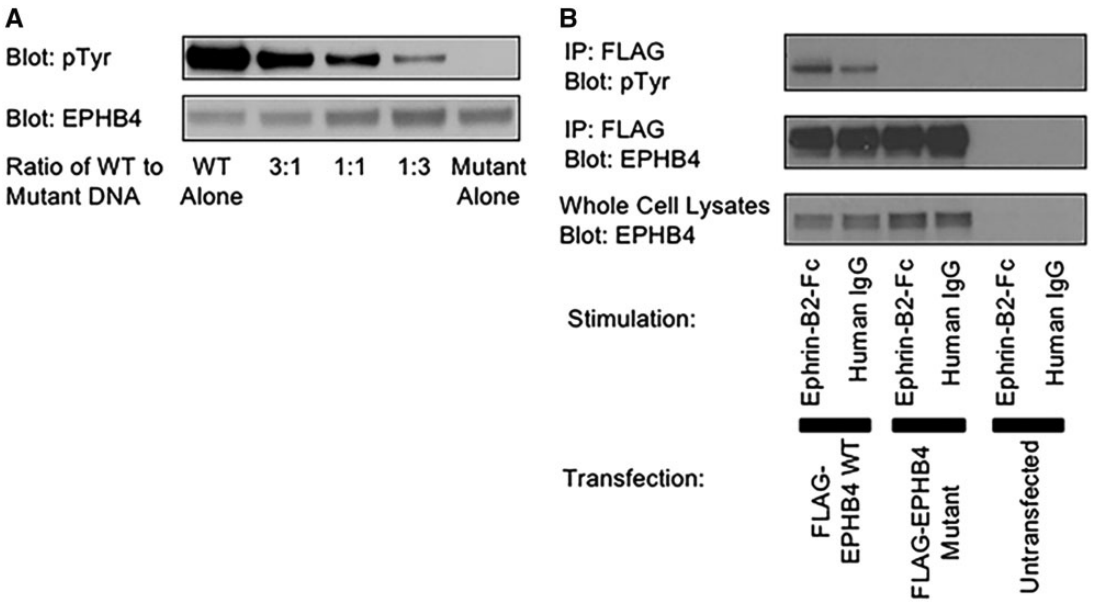

Figure 3. LoF mutation in *EPHB4*. (**A**) HEK293T cells were transiently transfected with wild-type *EPHB4* alone, mutant *EPHB4* alone or the mixtures of the wild-type and mutant in the indicated ratios. (**B**) A375 cells were transfected with wild-type *EPHB4*, mutant *EPHB4* or left untransfected. Cells were stimulated with either plate-bound Ephrin-B2-Fc or human IgG1 as a control. Cells were lysed, and transfected proteins were immunoprecipitated. IPs were blotted for phosphotyrosine (top) or EPHB4 (middle). Whole cell lysates were blotted for EPHB4 to demonstrate equal expression (bottom).

at 4 dpf, (Fig. 4C). Amplification of *ephb4a* cDNA derived from the morphants (MOPHs) revealed that specifically targeting the 13th exon resulted in cryptic splicing with either a small or larger insertion. Sanger sequencing showed that the smaller band was a 30-bp in-frame insertion (encoding VNTALVLSIL), while the larger band was due to the retention of the entire intron between exon 13 and 14 resulting in a premature stop codon (Supplementary Material, Fig. S1A).

To validate our observation, we designed another MO by inhibiting the translational start site (ATG). We observed similar lymphatic pattern in the resultant malformed vasculature (Supplementary Material, Fig. S1B–G). We also acquired the mutant line ephb4a^{sa11431} carrying a point nonsense mutation (p.Y67X) originally discovered by the Sanger Institute with the targeting induced local lesions in genomes (TILLING) approach (26). However, an in-cross of mutant carriers with the tg(fli1: EGFP) background did not show a defect in the caudal plexus or misbranching of intersomitic vessels. As the p.Y67X mutation occurred in the extracellular domain, which has no impact on receptor dimerization, we hypothesize that a second *ephb*4 gene in zebrafish, *ephb4b*, could compensate for the ephb4a function. Indeed, injection of an *ephb4b* MO (0.4 uM) targeting the exon 13 splice junction resulted in fusion and expansion of the caudal plexus at 54 hpf in 30.3% of multiple in-crosses zebrafish ($N = 99$) (Supplementary Material, Fig. S1H). At higher concentrations of MO (0.8 uM) ~70% of these larvae also developed vessel misbranching at 4 dpf (Supplementary Material, Fig. S1I and J). Interestingly, these phenotypes were not induced by the MO when only targeting *ephb4b* in wild-type larvae (Supplementary Material, Fig. S1K).

Both mTORC1 and MEK1/2 have been shown to be important signaling pathways regulating lymphatic development (27,28). These pathways are regulated by positive and negative feedback and cross-talk mechanisms (29). To determine if mTORC1 and MEK inhibitors could rescue the induced phenotypic and molecular changes observed in the MOPHs, we repeated the MO experiments in the presence and absence of the mTORC1 inhibitors, Rapamycin and BEZ235 (a dual PI-3-kinase and mTOR inhibitor), and the MEK inhibitors, U0126 and Cobimetinib, in separate experiments. Treatment with Rapamycin (24–54 hpf) resulted in a significant rescue of the defects in the caudal vascular plexus (>33.9%) in comparison with the untreated fishes (Fig. 4F; 6 experiments, 321 animals, $P = 0.01$). After Rapamycin treatment from 54 hpf to 4 dpf, substantial decrease in the intersomitic vessel misbranching was observed (>57.0%) in comparison with the untreated samples (Fig. 4G; 6 experiments, 136 animals, $P < 1E\text{-}04$). BEZ235 treatment from 54 hpf to 4 dpf rescued the defective vessel branching phenotype by 62.1% (Fig. 4H; 5 experiments, 159 animals, $P < 1E\text{-}04$). The MEK inhibitory drugs, U0126 and Cobimetinib, also similarly rescued the distorted vasculature induced by *ephb4a* MO by 66.9% (3 experiments, 111 animals, $P = 2E\text{-}04$) and 50.5% (3 experiments, 78 animals, $P = 0.02$), respectively (Fig. 4I and J).

Perturbations attributed to induced variants in *ephb4a* in developing zebrafish upregulate mTORC1 signaling, reversed by inhibitor therapy

To investigate the biochemical effects of the induced variants in *ephb4a* MOs, we lysed trunk section containing the affected vessels of multiple zebrafish larvae at 4.5 dpf, and analyzed the lysates for mTORC1 and MAPK pathways by western blot. Levels of phosphorylation were assessed in triplicate. Elevated mTORC1 signaling as evidenced by phosphorylation of both mTOR and its downstream target p70S6 kinase (p70S6K; an indicator of mTORC1 activation) was observed in *ephb4a* MOPHs (Fig. 5A). The activation of mTORC1 as illustrated by p70S6K was inhibited by treatment of the developing larvae with Rapamycin and BEZ235, while ERK1/2 showed consistently

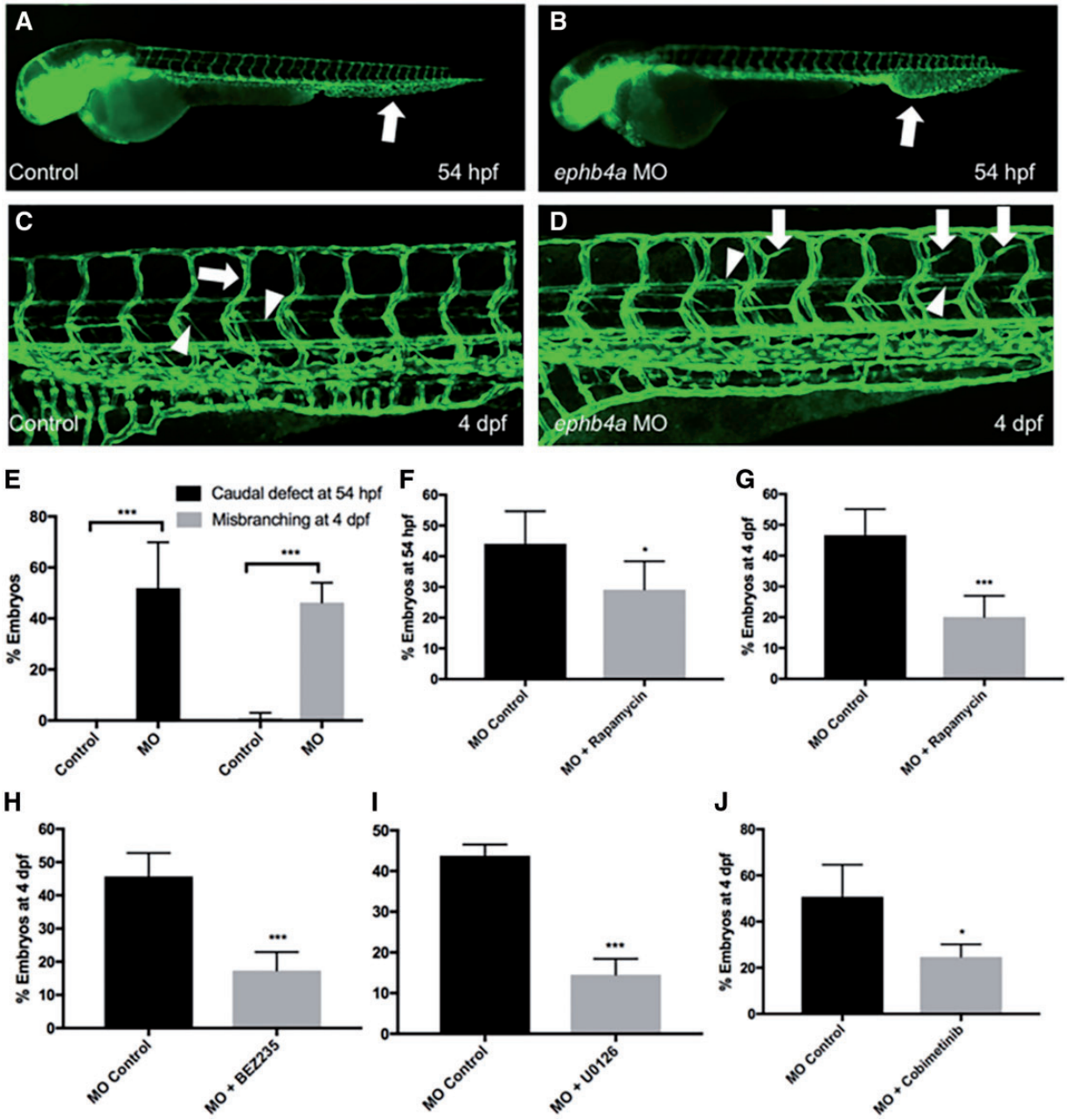

Figure 4. *ephb4a* MOs induces mTORC1 signaling-dependent expansion of the caudal vascular plexus and miss-guided vessels in the intersomitic vasculature. (**A** and **B**) Injection of *ephb4a* MO (800 uM) in the tg(fli1: EGFP) zebrafish line (in which endothelial cells is marked by EGFP expression) induces expansion and fusion of the caudal vasculature at 54 hpf (arrows). (**C**) At 4 dpf the zebrafish vascular system consists of intersomitic blood vessels that project in dorso-ventral direction (arrow) as well as thinner lymphatic vessels (arrowheads). The lymphatic parachordal line runs horizontally along the trunk (downward arrowhead) while the intersegmental lymphatic vessels project downwards (upward arrowhead). (**D**) *ephb4a* MO induces misguided vessels that resemble blood vessels (arrows) and lymphatic vessels (arrowheads). (Images of C and D are merged from two neighboring confocal scans) (**E**) The defects in the caudal plexus are detected in 52% of *ephb4a* MO-injected larvae at 54 hpf, misguided vasculature is present in 46% on day 4 (***$P < 0.001$). (**F** and **G**) Rapamycin can significantly reduce the number of animals with caudal defect and misbranching at 54 hpf (F, *$P < 0.05$) and 4 dpf (G, ***$P < 0.001$), respectively. (**H–J**) BEZ235 (H, ***$P < 0.001$), U0126 (I, ***$P < 0.001$) and Cobimetibib (J, *$P < 0.05$) similarly rescue the branching defects on day 4.

high constitutive activation as detected by phosphorylation level in all conditions (Fig. 5A). However, this ERK1/2 constitutive phosphorylation was downregulated by the treatment of an MEK inhibitory drug, U0126, in the *ephb4a* MO (Fig. 5B), suggesting both the PI3K/mTORC1 and RAS/EKR1/2 branches of intracellular signaling can independently control lymphatic development.

Knock-in of *EPHB4* mutation in HEK293T cells results in increased mTORC1 activity

We used CRISPR-Cas9 to generate a cellular model for *EPHB4* (Fig. 6A). The knock-in was confirmed by directly amplifying and sequencing genomic DNA and the exon 12–14 region of *EPHB4* cDNA (Fig. 6B–D). Western blot analysis of the

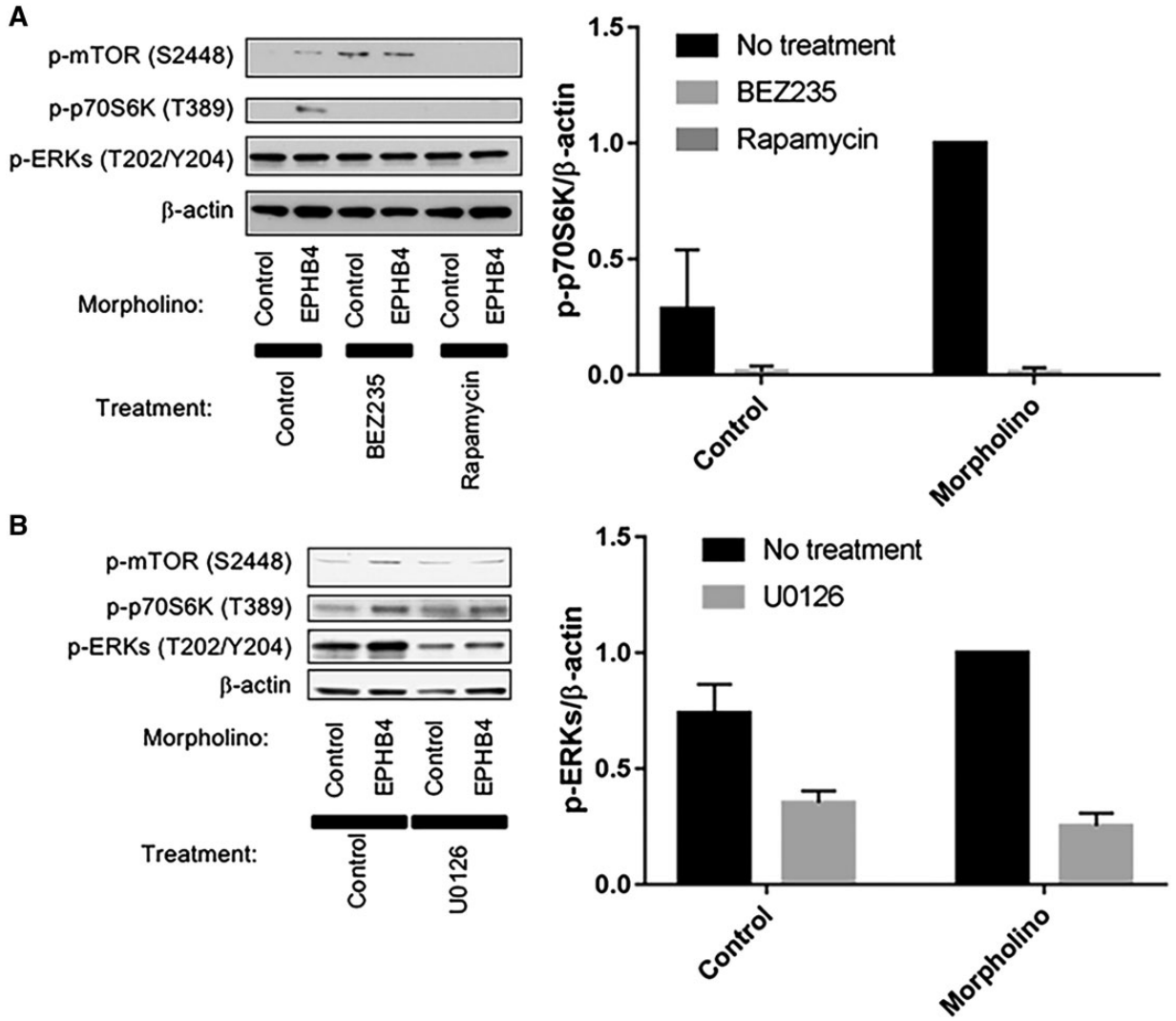

Figure 5. Perturbation attributed to *ephb4a* MO in developing zebrafish upregulate mTORC1 signaling and activation of mTORC1 can be inhibited by treatment of mTORC1 inhibitors. (**A** and **B**) Lysates from zebrafish larvae treated with either *ephb4a* MO or control MO, and untreated, or treated with Rapamycin or BEZ235 **(A)** or with U0126 (a MEK inhibitor) **(B)** were separated by SDS-PAGE and blotted for phospho-mTOR S2448, phospho-p70S6K T389 and phospho-ERKs. Blotting for β-actin was used as a loading control. Normalized quantification of p-p70S6K and p-ERKs against β-actin was performed from three independent experiments. Data are presented as mean ± SD.

gene-edited cells with the *EPHB4* splice-altering mutation displayed enhanced phosphorylation of p70S6K levels as compared with that of wild-type cells (Fig. 6E).

Discussion

The patients reported here are from a four-generation pedigree with a significant family history of venolymphatic dysfunction—edema of lower extremities, venous stasis and variable chylous effusion. The venous insufficiency doesn't fulfill the definition of venous malformation and lymphatic dysfunction observed in our family suggests a channel-type lymphatic malformation based on 2015 ISSVA classification of vascular anomalies (17). The advent of DCMRL, a new advanced imaging technique, allows better understanding of the anatomy and flow of the lymphatic system. Examination of image data showed that the proband has dilated thoracic duct and retrograde lymph flow into lung, which leads to pleural effusions and respiratory distress, further substantiating the validity of the CCLA diagnosis in this studied proband.

We obtained convincing evidence that an inherited germline mutation in *EPHB4* is responsible for the variable lymphatic anomaly phenotype in the six family members, whose clinical features were also notable for venous involvement and lack of bony involvement, which excludes the GLA diagnosis (30). *EPHB4* encodes for Ephrin B-type receptor 4, which is a receptor tyrosine kinase and recognizes Ephrin-B2 (EFNB2) as a specific ligand. In animal models the EFNB2/EPHB4 pathway has previously been shown to impact venous and lymphatic cell fate determination, and lymphatic valve development (31–34). Specifically, lymphatic vessel sprouting from the cardinal vein requires cell migration to penetrate the surrounding tissue to be correctly positioned. This cellular migration is controlled by repulsive forward Ephb4 signal when encountering a cell with Efnb2 (35). So cells lacking EPHB4 signal, rather than stopping at the correct positions, keep getting pro-migration signals from

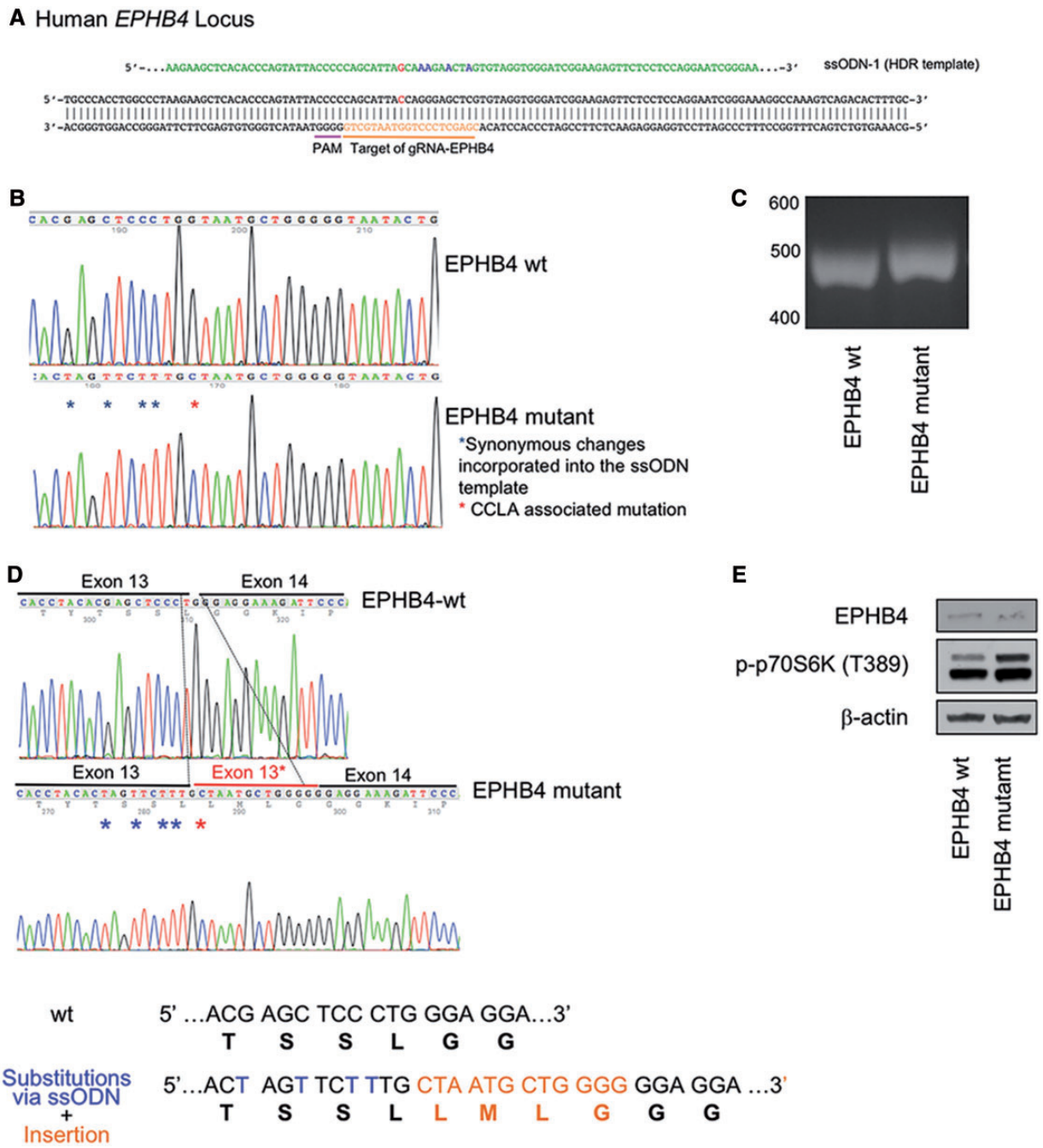

Figure 6. Knock-in of *EPHB4* mutation in HEK293T cells results in increased mTORC1 activity. (**A**) Schematic drawing of targeted genome editing at *EPHB4* locus using CRISPR/Cas9. (**B**) Sanger sequence traces of genomic DNA after the knock-in. (**C**) RT-PCR analysis suggested a small insertion in the knock-in cells compare with the wild-type cells. (**D**) The four-amino-acid insertion induced by CRISPR/Cas9 confirmed by standard Sanger sequencing of RT-PCR product. (**E**) Western blot of the wild-type HEK293T cells and EPHB4 mutant cells by gene editing. Cells containing the EPHB4 splice-altering mutation displayed higher p-p70S6K levels than wild-type cells.

their environment, which leads to abnormal lymphatic branching. We have shown that the mutation c.2334+1G>C in *EPHB4* leads to in-frame insertion (p.L778_G779insLMLG) in the protein kinase domain, which participates in phosphorylation in forward signaling. Indeed, our functional data both validate the pathogenicity of this mutation and show the insertion decreases the phosphorylation state of the EPHB4 protein. Furthermore, modeling the splice-altering mutation in zebrafish results in disorganized blood and lymphatic vasculature, indicative of possibly differentiation defects both in blood and lymphatic vessels and mimicking the presentations of the patients. Strikingly, drugs that inhibit mTOR or MAPK signaling were both able to rescue the disorganized lymphatics through rectifying the over-activation of mTORC1 signaling by mTOR inhibitory drugs and downregulating MAPK signaling by MEK inhibitory drugs. Although it's controversial whether ERK is

proximal downstream target of EPHB4 signaling, our data suggest both pathways can independently control lymphatic fate specification. While this work was in progress, two families with history of nonimmune hydrops fetalis were reported with germline heterozygous missense variants located in the protein kinase domain of *EPHB4* (19). Most recently, mutations in *EPHB4* have been described in two additional distinct clinical disease entities—capillary malformation-arteriovenous malformation and vein of Galen aneurysmal malformation (36). Despite harboring a similar LoF genetic defect, there is considerable variability in terms of expressivity and penetrance, suggesting that other modifying genetic and/or environmental factors are at play. Taken together, our work demonstrates that LoF *EPHB4* mutations result in a widespread vascular disorder.

Until recently, sclerotherapy and surgical resection and embolization techniques were the only treatments for some lymphatic anomalies and in others there was no effective treatment, but now mTOR inhibitors have become a possible treatment option in management of some lymphatic anomalies, including GLA, Gorham-Stout syndrome, kaposiform lymphagiomatosis and venous lymphatic malformation (37–39). Although the majority of patients were reported to partially respond to sirolimus (a.k.a. Rapamycin) treatment, treatment response is still inconsistent suggesting genetic heterogeneity beyond the mTOR pathway in these disorders or upstream feedback mechanisms that reactivate this pathway. Our treatment of *ephb4a* MO with preclinical PI3K/mTORC1 or RAS/MAPK inhibitory drugs dramatically restored the normal vessel architecture, suggesting a possible avenue for direct therapeutic intervention by the inhibitory drugs in both pathways.

In summary we report here a kinase-inactivating mutation (c.2334+1G>C: p.L778_G779insLMLG) in the *EPHB4* gene that follows an autosomal dominant mode of inheritance with variable expression as the cause of clinical presentations in the six affected family members, representing the first report of an autosomal dominant form of CCLA and a potential avenue for therapeutic intervention for related complex lymphatic anomalies.

Materials and Methods

Whole exome sequencing and bioinformatics analysis

Exons were captured from qualified fragmented genomic DNA samples using the SureSelect Human All Exon 51 Mb kit (Agilent Technologies, Santa Clara, California, USA). Paired-end 101-base massively parallel sequencing was carried out on the Illumina HiSeq2500 platform (Illumina, San Diego, California, USA) in Center for Applied Genomics, according to the manufacture's protocols. Base calling was performed by the Illumina CASAVA software (version 1.8.2) with default parameters. Sequencing reads passing the quality filter were aligned to the human reference genome (GRCh37-derived alignment set used in 1000 Genomes Project) with Burrows-Wheeler Aligner (BWA, v.0.7.12) (40). PCR duplicates were removed using Picard (v.1.97). The Genome Analysis Toolkit (GATK, v.2.6–5) was used to generate variant calls (41). All variants were then annotated by ANNOVAR (42) and SnpEff (v.2.0.5) (43) to collect amino acid change, protein functional effect, conservation score, minor allele frequency (MAF) and output from prediction programs (SIFT, Polyphen2, LRT and MutationTaster). We examined missense, nonsense, splice-altering and coding indels matching the dominant mode of inheritance in the exome data. Results were filtered to exclude synonymous variants, variants with MAF greater than 0.5%, and variants previously identified in controls by our in-house exome variant database (20,21). To facilitate identification of dominant variants, we presumed that the variants responsible for the disease would be rare and probably absent in the general population. The dominant variants identified were then further filtered to exclude variants that had more than five occurrences in gnomAD. Subsequent gene prioritization was on basis of deleterious predication and biology relevance by referring to Online Mendelian Inheritance in Man (OMIM). Validation of surviving candidates was performed by standard Sanger sequencing.

RNA-Seq

RNA from the skin biopsies obtained from the lead proband was extracted using the AllPrep DNA/RNA Mini Kit (Qiagen). Extracted RNA samples underwent quality control assessment using R6K Screen Tape on a 2200 Tape Station (Agilent) and were quantified using Qubit 2.0 Fluorimeter from Life Technologies (Grand Island, NY). Strand-specific RNA library was prepared from 100 ng total RNA using the Encore Complete RNA-Seq library kit (Nugen Technologies, Inc., San Carlos, CA, USA) according to the manufacturer's protocol. Briefly, non-rRNA-enriched cDNA was prepared and converted to libraries with adaptors and reagents provided in the kit. The library quality was assessed by qPCR using Kappa Library Quant kit (Kappa Biosystems, Woburn, MA, USA). RNA sequencing was performed on the Illumina HiSeq2500 platform (Illumina), per standard protocols. The RNA-Seq data were aligned to the hg19 reference genome using STAR (44) with default parameters. Transcripts were assembled using Cufflinks software (45).

Expression and characterization of *EPHB4* mutation in mammalian cell lines

A plasmid containing the *EPHB4* coding sequence was obtained from GE Dharmacon (cat# MHS6278–202833446, Lafayette, CO). The discovered 12-base-pair insertion was made via the Quikchange II mutagenesis kit (Agilent) using primers: 5′-TGGGAATCTTTCCTCCCCCCAGCATTAGCAGGGAGCTAGTGTAG-3′ and 5′-CTACACTAGCTCCCTGCTAATGCTGGGGGGAGGAAAGA TTCCCA-3′. The coding sequence was amplified by PCR using forward primer 5′-ATGAATTCGCCACCATGGAGCTCCGGGTGCT GCTC-3′ and reverse primer 5′-ATGCGGCCGCTCAGTACTGCGG GGCCGGTCC-3′ and ligated into the *Eco*RI and *Not*I sites of pBABE-CMV-Puro (46). A FLAG tag was inserted into the coding sequence following the signal peptide via the Q5 Mutagenesis kit (NEB, Ipswich, MA) using the forward primer 5′-GATGATGAT AAATTGGAAGAGACCCTGCTGAACAC-3′ and the reverse primer 5′-ATCTTTATAATCAGCTGCAGCCAACGAAGC-3′. All sequences were confirmed by Sanger sequencing. Wild-type and mutant cDNA were transfected into HEK293T or A375 melanoma cell lines. We measured the phosphorylation levels by means of western blot analysis.

Transfection and stimulation of EPHB4

HEK293T cells and the A375 melanoma cell line were obtained from ATCC (Manassas, VA). Transfections were performed using Fugene HD (Promega, Madison, WI), with 3 μg DNA and 9 μl of the transfection reagent, according to manufacturer's protocols. For stimulation of transfected cells, 6-well plates (not tissue culture treated, Thermo Scientific) were coated overnight at 37°C

with either Ephrin-B2-Fc (cat# 7397-EB, R&D Systems) or IgG1, kappa from human myeloma plasma (cat# I5154, Sigma, St. Louis, MO) at 5 μg/ml in 50 mM sodium carbonate solution (pH 9.6). Plates were washed with PBS, blocked with 1% BSA in PBS for 30 min at 4°C, and washed again with PBS. Transfected cells were removed from their plates using 10 mM EDTA in DMEM, washed and resuspended in serum-free DMEM, and added to coated plates. Plates were placed at 4°C for 15 min and moved to 37°C for 20 min, after which cells were lysed. Where indicated, FLAG immunoprecipitations (IPs) were performed using Anti-FLAG M2 Affinity Gel (cat# A2220, Sigma). IPs and lysates were run on NuPAGE 4–12% Bis–Tris gels and blotted with anti-phosphotyrosine—4G10-Biotin (cat# 16–103, EMD Millipore, Billerica MA) and anti-EPHB4 (cat# AF3038, R&D Systems, Minneapolis, MN).

Zebrafish morpholino experiment

All procedures using zebrafish were approved by the Institutional Animal Care and Use Committee of the Children's Hospital of Philadelphia (IAC 001154) and were in accordance with Guide for the Care and Use of Laboratory Animals by the National Institutes of Health. Zebrafish larvae were raised in E3 medium containing 0.03 mg/ml PTU at 28°C. Zebrafish were anesthetized in approximate 0.1 mg/ml Tricaine (E3). Vascular and lymphatic endothelial cells were visualized using the tg(fli1: EGFP) line (24). MOs (Gene Tools, OR) were diluted in water and heated to 65°C for 5 min before injection as suggested by the manufacturer. Drop size was adjusted to 0.120 mm diameter (905 pl volume), and MOs were injected in the middle of the yolk of 1-cell stage embryos.

ephb4a ATG: 5′-GCGGAATCACGAGTGTTTTACTTGT-3′, injected at 0.75 mM

ephb4a exon 13: 5′-CGAGAGCAGTATTTACCAGTGAGCT-3′, injected at 0.8 mM

ephb4b exon 13: 5′-TCTGAAAGAGCAGCTTCTCACCAGT-3′, injected at 0.8 mM

Standard control oligo: 5′-CCTCTTACCTCAGTTACAATTT ATA-3′, injected at 0.5 mM

Microscopy

Fluorescent and bright field images were taken on an Olympus MVX10 dissecting scope equipped with an Olympus DP73 camera. High magnifications images were taken with an Olympus BX63 microscope with a Hamamatsu Ocra Flash 4 camera. Confocal scans were performed using a Zeiss LSM710 confocal microscope. Confocal z-stacks of images were superimposed using Zeiss Zen software's maximum intensity projection function. Frequently two neighboring panels were combined in one image.

For regular imaging zebrafish larvae were mounted on a layer of 3% methyl cellulose, for confocal imaging larvae were imbedded in 1% low melting arose as described previously (47,48). Images were compiled in ImageJ (Fiji) (49), Affinity Photo (Serif) and PowerPoint (Microsoft).

Validation of morpholino efficiency

RNA was extracted using the Nucleospin RNAeasy kit (Clontech), cDNA was synthesized with Superskript III (Invitrogen) according to manufacturer's instruction using equal amounts of RNA in reaction groups. For PCR, High Fidelity Platinum Taq polymerase (Invitrogen) was used. One-step RT-PCR/PCR was performed using FideliTaq (Affymetrix/USB, CA).

Treatment with inhibitory drugs

Drug treatments were performed in 6-well plates with up to 20 larvae per group. For tail vessel expansion phenotypes larvae were treated from 24 hpf and imaged at 54 hpf for MO-injected or transient transgenic treated zebrafish. For vessel branching analysis larvae were treated from 54 hpf and analyzed at 4 dpf. Drugs were diluted in embryo medium (as described above) containing 0.01 M Tris pH 7.2 and 0.1% DMSO. Rapamycin was used at 0.4 uM, BEZ235 at 100 nM, U0126 at 50 uM, Selumetinib at 100 uM, Cobimetinib at 250 nM and DMSO (0.1%) as control.

Western blotting of zebrafish lysates

Trunk sections of zebrafish larvae at 4.5 dpf were lysed in radioimmunoprecipitation assay (RIPA) buffer supplemented with protease inhibitors (complete protease inhibitor cocktail tablets, Roche, Mannheim, Germany). Approximately 5 micrograms of protein were separated on NuPAGE 4–12% Bis–Tris gels run with MOPS SDS running buffer (Life Technologies, Carlsbad, CA). Western blot was performed using the following antibodies as described above: p-p70S6K T389 (cat# 9205S, Cell Signaling, Danvers, MA), anti-phospho-p70S6K T389, anti-phospho-mTOR Ser2448, anti-phospho-ERKs T202/Y204 and anti-β-actin.

CRISPR/Cas9 design and synthesis

We co-transfect pSpCas9(BB)-2A-Puro vector containing the specific target sequence for *EPHB4* locus (gRNA-EPHB4) and a single-stranded donor oligonucleotides (ssODN) into HEK293T cells using the Lipofectamine 2000 transfection reagent per manufacturer's instructions. ssODN contains a single base mismatch to the genomic sequence to recreate the EPHB4 splice-altering mutation and four synonymous changes. pSpCas9(BB)-2A-Puro (PX459) V2.0 was purchased from Addgene (Plasmid ID# 62988) (50). The gRNAs used in this study (ggtcgtaatggtccctcga for *EPHB4*) is present immediately upstream of a Protospacer Adjacent Motif (PAM) and were designed using the gRNA designer from MIT (http://crispr.mit.edu/). For gRNAs assembly, a pair of synthesized oligos for each targeting site with the following sequence (hEPHB4-F-5′-caccgCGAGCTCCCTGGTAATGCTG-3′, hEPHB4-R-5′-aaacCAGCATTACCAGGGAGCTCGc-3′) were annealed and paste in pSpCas9(BB)-2A-Puro using BbsI (NEB) restriction enzyme site.

The synthesized ssODNs (180 bases) were purchased from IDT: hEPHB4 ssODN: 5′-accctcagcctcccacctttccaacctgccctgcccacc tggccctaagaagctcacacccagtattacccccagcattagcaaagaactagtgtaggt gggatcggaagagttctcctccaggaatcgggaaaggccaaagtcagacactttgcaga cgaggttgctgttgactagga-3′.

Supplementary Material

Supplementary Material is available at *HMG* online.

Acknowledgements

We thank the family members involved in this study. We acknowledge Dr Cameron C. Trenor III (Boston Children's Hospital), Dr Ahmad Alomari (Boston Children's Hospital) and

Dr Miikka Vikkula (Université Catholique de Louvain) for their insightful comments on the reported proband. Research reported in this publication was supported by an anonymous donation [to H.H. and Center for Applied Genomics (CAG)] from a family supporting lymphatic anomaly research (which initiated the project), the Institutional Development Funds (to H.H.) from The Children's Hospital of Philadelphia (CHOP) and donation from the Adele and Daniel Kubert family (to H.H. and CAG). The study was also funded in part through a sponsored research agreement from Aevi Genome Medicine Inc., funding discovery and translation of rare and orphan disease genes at the CAG.

Conflict of Interest statement. Dr Hakonarson is a scientific advisor to Aevi Genome Medicine Inc. and he indirectly owns shares of the company. Other authors have nothing to disclose.

References

1. Alitalo, K., Tammela, T. and Petrova, T.V. (2005) Lymphangiogenesis in development and human disease. *Nature*, **438**, 946–953.
2. Adams, R.H. and Alitalo, K. (2007) Molecular regulation of angiogenesis and lymphangiogenesis. *Nat. Rev. Mol. Cell. Biol.*, **8**, 464–478.
3. Tammela, T. and Alitalo, K. (2010) Lymphangiogenesis: molecular mechanisms and future promise. *Cell*, **140**, 460–476.
4. Alitalo, K. (2011) The lymphatic vasculature in disease. *Nat. Med.*, **17**, 1371–1380.
5. Brouillard, P., Boon, L. and Vikkula, M. (2014) Genetics of lymphatic anomalies. *J. Clin. Invest.*, **124**, 898–904.
6. Kurek, K.C., Luks, V.L., Ayturk, U.M., Alomari, A.I., Fishman, S.J., Spencer, S.A., Mulliken, J.B., Bowen, M.E., Yamamoto, G.L., Kozakewich, H.P. *et al.* (2012) Somatic mosaic activating mutations in PIK3CA cause CLOVES syndrome. *Am. J. Hum. Genet.*, **90**, 1108–1115.
7. Lindhurst, M.J., Sapp, J.C., Teer, J.K., Johnston, J.J., Finn, E.M., Peters, K., Turner, J., Cannons, J.L., Bick, D., Blakemore, L. *et al.* (2011) A mosaic activating mutation in AKT1 associated with the Proteus syndrome. *N. Engl. J. Med.*, **365**, 611–619.
8. Luks, V.L., Kamitaki, N., Vivero, M.P., Uller, W., Rab, R., Bovee, J.V., Rialon, K.L., Guevara, C.J., Alomari, A.I., Greene, A.K. *et al.* (2015) Lymphatic and other vascular malformative/overgrowth disorders are caused by somatic mutations in PIK3CA. *J. Pediatr.*, **166**, 1048–1054.e1-5.
9. Lo, I.F., Brewer, C., Shannon, N., Shorto, J., Tang, B., Black, G., Soo, M.T., Ng, D.K., Lam, S.T. and Kerr, B. (2008) Severe neonatal manifestations of Costello syndrome. *J. Med. Genet.*, **45**, 167–171.
10. Fabretto, A., Kutsche, K., Harmsen, M.B., Demarini, S., Gasparini, P., Fertz, M.C. and Zenker, M. (2010) Two cases of Noonan syndrome with severe respiratory and gastroenteral involvement and the SOS1 mutation F623I. *Eur. J. Med. Genet.*, **53**, 322–324.
11. Joyce, S., Gordon, K., Brice, G., Ostergaard, P., Nagaraja, R., Short, J., Moore, S., Mortimer, P. and Mansour, S. (2016) The lymphatic phenotype in Noonan and Cardiofaciocutaneous syndrome. *Eur. J. Hum. Genet.*, **24**, 690–696.
12. Morcaldi, G., Bellini, T., Rossi, C., Maghnie, M., Boccardo, F., Bonioli, E. and Bellini, C. (2015) Lymphodysplasia and KRAS mutation: a case report and literature review. *Lymphology*, **48**, 121–127.
13. Pandit, B., Sarkozy, A., Pennacchio, L.A., Carta, C., Oishi, K., Martinelli, S., Pogna, E.A., Schackwitz, W., Ustaszewska, A., Landstrom, A. *et al.* (2007) Gain-of-function RAF1 mutations cause Noonan and LEOPARD syndromes with hypertrophic cardiomyopathy. *Nat. Genet.*, **39**, 1007–1012.
14. Razzaque, M.A., Nishizawa, T., Komoike, Y., Yagi, H., Furutani, M., Amo, R., Kamisago, M., Momma, K., Katayama, H., Nakagawa, M. *et al.* (2007) Germline gain-of-function mutations in RAF1 cause Noonan syndrome. *Nat. Genet.*, **39**, 1013–1017.
15. Trenor, C.C., 3rd and Chaudry, G. (2014) Complex lymphatic anomalies. *Semin. Pediatr. Surg.*, **23**, 186–190.
16. Clemens, R.K., Pfammatter, T., Meier, T.O., Alomari, A.I. and Amann-Vesti, B.R. (2015) Combined and complex vascular malformations. *Vasa*, **44**, 92–105.
17. Wassef, M., Blei, F., Adams, D., Alomari, A., Baselga, E., Berenstein, A., Burrows, P., Frieden, I.J., Garzon, M.C., Lopez-Gutierrez, J.C. *et al.* (2015) Vascular anomalies classification: recommendations from the international society for the study of vascular anomalies. *Pediatrics*, **136**, e203–e214.
18. Amyere, M., Revencu, N., Helaers, R., Pairet, E., Baselga, E., Cordisco, M., Chung, W., Dubois, J., Lacour, J.P., Martorell, L. *et al.* (2017) Germline loss-of-function mutations in EPHB4 cause a second form of capillary malformation-arteriovenous malformation (CM-AVM2) deregulating RAS-MAPK signaling. *Circulation*, **136**, 1037–1048.
19. Martin-Almedina, S., Martinez-Corral, I., Holdhus, R., Vicente, A., Fotiou, E., Lin, S., Petersen, K., Simpson, M.A., Hoischen, A., Gilissen, C. *et al.* (2016) EPHB4 kinase-inactivating mutations cause autosomal dominant lymphatic-related hydrops fetalis. *J. Clin. Invest.*, **126**, 3080–3088.
20. Li, D., Yuan, H., Ortiz-Gonzalez, X.R., Marsh, E.D., Tian, L., McCormick, E.M., Kosobucki, G.J., Chen, W., Schulien, A.J., Chiavacci, R. *et al.* (2016) GRIN2D recurrent de novo dominant mutation causes a severe epileptic encephalopathy treatable with NMDA receptor channel blockers. *Am. J. Hum. Genet.*, **99**, 802–816.
21. Li, D., Tian, L., Hou, C., Kim, C.E., Hakonarson, H. and Levine, M.A. (2016) Association of mutations in SLC12A1 encoding the NKCC2 cotransporter with neonatal primary hyperparathyroidism. *J. Clin. Endocrinol. Metab.*, **101**, 2196–2200.
22. Kuijper, S., Turner, C.J. and Adams, R.H. (2007) Regulation of angiogenesis by Eph-ephrin interactions. *Trends Cardiovasc. Med.*, **17**, 145–151.
23. Heroult, M., Schaffner, F., Pfaff, D., Prahst, C., Kirmse, R., Kutschera, S., Riedel, M., Ludwig, T., Vajkoczy, P., Graeser, R. *et al.* (2010) EphB4 promotes site-specific metastatic tumor cell dissemination by interacting with endothelial cell-expressed ephrinB2. *Mol. Cancer Res.*, **8**, 1297–1309.
24. Lawson, N.D. and Weinstein, B.M. (2002) In vivo imaging of embryonic vascular development using transgenic zebrafish. *Dev. Biol.*, **248**, 307–318.
25. Mulligan, T.S. and Weinstein, B.M. (2014) Emerging from the PAC: studying zebrafish lymphatic development. *Microvasc. Res.*, **96**, 23–30.
26. Kettleborough, R.N., Busch-Nentwich, E.M., Harvey, S.A., Dooley, C.M., de Bruijn, E., van Eeden, F., Sealy, I., White, R.J., Herd, C., Nijman, I.J. *et al.* (2013) A systematic genome-wide analysis of zebrafish protein-coding gene function. *Nature*, **496**, 494–497.
27. Sun, S., Chen, S., Liu, F., Wu, H., McHugh, J., Bergin, I.L., Gupta, A., Adams, D. and Guan, J.L. (2015) Constitutive activation of mTORC1 in endothelial cells leads to the development and progression of lymphangiosarcoma through VEGF autocrine signaling. *Cancer Cell*, **28**, 758–772.

28. Deng, Y., Atri, D., Eichmann, A. and Simons, M. (2013) Endothelial ERK signaling controls lymphatic fate specification. *J. Clin. Invest.*, **123**, 1202–1215.
29. Mendoza, M.C., Er, E.E. and Blenis, J. (2011) The Ras-ERK and PI3K-mTOR pathways: cross-talk and compensation. *Trends Biochem. Sci.*, **36**, 320–328.
30. Lala, S., Mulliken, J.B., Alomari, A.I., Fishman, S.J., Kozakewich, H.P. and Chaudry, G. (2013) Gorham-Stout disease and generalized lymphatic anomaly–clinical, radiologic, and histologic differentiation. *Skeletal Radiol.*, **42**, 917–924.
31. Makinen, T., Adams, R.H., Bailey, J., Lu, Q., Ziemiecki, A., Alitalo, K., Klein, R. and Wilkinson, G.A. (2005) PDZ interaction site in ephrinB2 is required for the remodeling of lymphatic vasculature. *Genes Dev.*, **19**, 397–410.
32. Kume, T. (2010) Specification of arterial, venous, and lymphatic endothelial cells during embryonic development. *Histol. Histopathol.*, **25**, 637–646.
33. Hashimoto, T., Tsuneki, M., Foster, T.R., Santana, J.M., Bai, H., Wang, M., Hu, H., Hanisch, J.J. and Dardik, A. (2016) Membrane-mediated regulation of vascular identity. *Birth Defects Res. C Embryo Today*, **108**, 65–84.
34. Zhang, G., Brady, J., Liang, W.C., Wu, Y., Henkemeyer, M. and Yan, M. (2015) EphB4 forward signalling regulates lymphatic valve development. *Nat. Commun.*, **6**, 6625.
35. Fuller, T., Korff, T., Kilian, A., Dandekar, G. and Augustin, H.G. (2003) Forward EphB4 signaling in endothelial cells controls cellular repulsion and segregation from ephrinB2 positive cells. *J. Cell Sci.*, **116**, 2461–2470.
36. Vivanti, A., Ozanne, A., Grondin, C., Saliou, G., Quevarec, L., Maurey, H., Aubourg, P., Benachi, A., Gut, M., Gut, I. *et al.* (2018) Loss of function mutations in EPHB4 are responsible for vein of Galen aneurysmal malformation. *Brain*, **141**, 979–988.
37. Lackner, H., Karastaneva, A., Schwinger, W., Benesch, M., Sovinz, P., Seidel, M., Sperl, D., Lanz, S., Haxhija, E., Reiterer, F. *et al.* (2015) Sirolimus for the treatment of children with various complicated vascular anomalies. *Eur. J. Pediatr.*, **174**, 1579–1584.
38. Adams, D.M., Trenor, C.C., 3rd, Hammill, A.M., Vinks, A.A., Patel, M.N., Chaudry, G., Wentzel, M.S., Mobberley-Schuman, P.S., Campbell, L.M., Brookbank, C. *et al.* (2016) Efficacy and safety of sirolimus in the treatment of complicated vascular anomalies. *Pediatrics*, **137**, e20153257.
39. Triana, P., Dore, M., Cerezo, V.N., Cervantes, M., Sanchez, A.V., Ferrero, M.M., Gonzalez, M.D. and Lopez-Gutierrez, J.C. (2017) Sirolimus in the treatment of vascular anomalies. *Eur. J. Pediatr. Surg.*, **27**, 86–90.
40. Li, H. and Durbin, R. (2009) Fast and accurate short read alignment with Burrows-Wheeler transform. *Bioinformatics*, **25**, 1754–1760.
41. DePristo, M.A., Banks, E., Poplin, R., Garimella, K.V., Maguire, J.R., Hartl, C., Philippakis, A.A., del Angel, G., Rivas, M.A., Hanna, M. *et al.* (2011) A framework for variation discovery and genotyping using next-generation DNA sequencing data. *Nat. Genet.*, **43**, 491–498.
42. Wang, K., Li, M. and Hakonarson, H. (2010) ANNOVAR: functional annotation of genetic variants from high-throughput sequencing data. *Nucleic Acids Res.*, **38**, e164.
43. Cingolani, P., Platts, A., Wang le, L., Coon, M., Nguyen, T., Wang, L., Land, S.J., Lu, X. and Ruden, D.M. (2012) A program for annotating and predicting the effects of single nucleotide polymorphisms, SnpEff: SNPs in the genome of *Drosophila melanogaster* strain w1118; iso-2; iso-3. *Fly (Austin)*, **6**, 80–92.
44. Dobin, A., Davis, C.A., Schlesinger, F., Drenkow, J., Zaleski, C., Jha, S., Batut, P., Chaisson, M. and Gingeras, T.R. (2013) STAR: ultrafast universal RNA-seq aligner. *Bioinformatics*, **29**, 15–21.
45. Trapnell, C., Hendrickson, D.G., Sauvageau, M., Goff, L., Rinn, J.L. and Pachter, L. (2013) Differential analysis of gene regulation at transcript resolution with RNA-seq. *Nat. Biotechnol.*, **31**, 46–53.
46. Cohen, G.B., Gandhi, R.T., Davis, D.M., Mandelboim, O., Chen, B.K., Strominger, J.L. and Baltimore, D. (1999) The selective downregulation of class I major histocompatibility complex proteins by HIV-1 protects HIV-infected cells from NK cells. *Immunity*, **10**, 661–671.
47. Seiler, C., Gebhart, N., Zhang, Y., Shinton, S.A., Li, Y.S., Ross, N.L., Liu, X., Li, Q., Bilbee, A.N., Varshney, G.K. *et al.* (2015) Mutagenesis screen identifies agtpbp1 and eps15L1 as essential for T lymphocyte development in zebrafish. *PLoS One*, **10**, e0131908.
48. Seiler, C., Davuluri, G., Abrams, J., Byfield, F.J., Janmey, P.A. and Pack, M. (2012) Smooth muscle tension induces invasive remodeling of the zebrafish intestine. *PLoS Biol.*, **10**, e1001386.
49. Schindelin, J., Arganda-Carreras, I., Frise, E., Kaynig, V., Longair, M., Pietzsch, T., Preibisch, S., Rueden, C., Saalfeld, S., Schmid, B. *et al.* (2012) Fiji: an open-source platform for biological-image analysis. *Nat. Methods*, **9**, 676–682.
50. Ran, F.A., Hsu, P.D., Wright, J., Agarwala, V., Scott, D.A. and Zhang, F. (2013) Genome engineering using the CRISPR-Cas9 system. *Nat. Protoc.*, **8**, 2281–2308.